Study of the star formation rate bimodality in SDSS galaxies at low redshift

Marco Bianchi
University of Milano-Bicocca, Physics Department, Astrophysics and Space Physics master degree
Laboratory of Data Analysis 2023-2024, group 5: M. Bellotti, M. Bianchi, L. Carbone, and F. Leto di Priolo

22 July 2024

ABSTRACT

Galaxies at low redshift display a bimodality in their specific star formation rate (sSFR). This phenomenon is related to several factors, including (1) the accretion processes that drive galaxy growth, (2) the feedback processes that eject gas from galaxies, and (3) the interactions between galaxies and their surrounding environment. These processes are strongly influenced by key physical properties of galaxies, such as gas mass, stellar mass, and age. Therefore, it is possible to build models that describe the time evolution of sSFR based on these simple quantities.

We developed two very simple analytical models, based on strong assumptions, and applied them to a subset of the Sloan Digital Sky Survey (SDSS) dataset with $z < 0.08$. Our findings indicate that young, actively star-forming galaxies can be described by an open-box model at equilibrium, while old, passive galaxies are better represented by a closed-box model, which does not exchange gas with the surrounding halo. Then, we relaxed some assumptions, such as the equilibrium of the open-box model, by numerically integrating the differential equation of the model over infinitesimal time steps, obtaining improved results.

1 INTRODUCTION

Galaxies are the fundamental building blocks of the universe at cosmological scales. Therefore, understanding how they form, evolve over time, and interact, creating complex structures, is crucial for advancing our knowledge about the universe and its history. However, capturing the extreme diversity of galaxies in a mathematical model is a very challenging task.

In this context, it is well known (e.g., Kauffmann et al. 2003a) that two main populations can be identified in the plane of specific star formation rate (sSFR) versus stellar mass ($M_{\rm star}$): one of young, actively star-forming galaxies (the *main sequence*) and the other of old, mostly passive galaxies, as shown in Fig. 1. For this reason, a model relating sSFR and $M_{\rm star}$ should have at least two regimes, with a sharp transition past some threshold. In this work, we investigate the processes that either stimulate or quench the formation of new stars within galaxies at low redshift, and we try to develop simple mathematical models to test our assumptions.

The raw material for star formation is gas, which, under appropriate conditions, can collapse and form virialized objects. The amount of gas within a galaxy is not constant and is subject to a myriad of processes that depend on the main physical properties of the galaxy, such as age and mass. Therefore, we expect the sSFR to drop whenever the consumed gas is no longer replaced by new gas, coming either from stars (winds, supernovae) or from outside the galaxy.

In particular, gas inflow is strongly related to the properties of the dark matter halo that hosts the galaxy. This halo accretes matter from the intergalactic medium, a fraction $f_{\rm gas}$ of which is gas, typically at very high temperature. Such hot gas has very strong pressure support that prevents it from accreting onto the galaxy. Therefore, the gas must cool down before it can infall, i.e., the condition $\tau_{\rm cooling} < \tau_{\rm free\text{-}fall}$ is required. This condition can be translated into a requirement on halo mass (for details, see chapter 8.4 of Mo et al. (2010)). We make the following conservative assumption to have effective cooling:

$$M_{\rm halo} \in \left(M_{\rm halo,min} = 10^9 M_\odot\,,\; M_{\rm halo,max} = 10^{11.6} M_\odot\right), \qquad (1)$$

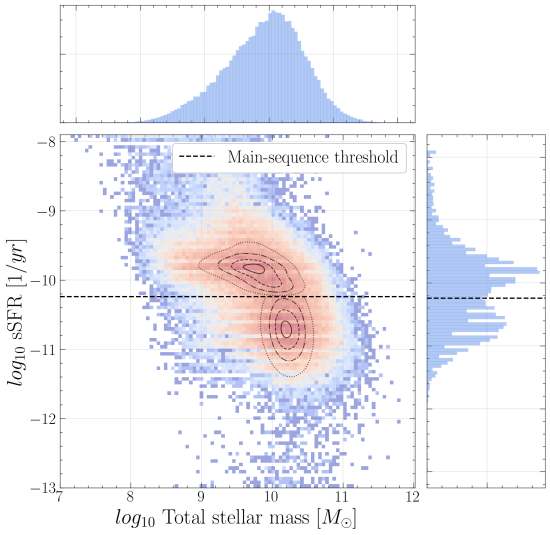

Figure 1. The main panel shows a 2D histogram of sSFR versus $M_{\rm star}$ for our dataset. The side panels display the marginal distributions of the two axes. The black dashed line indicates the value where the sSFR distribution has a local minimum, which is used to separate the main sequence from passive galaxies. The 25, 50, 75, and 95% contours of both populations are shown.

On the other hand, gas can also be expelled from the galaxy due to various processes, such as supernovae, AGN emission, and ram-pressure stripping. For simplicity, we will assume that Type IIA supernovae are the only sources of gas outflow, given their dominant role. However, not all gas expelled by supernovae gains enough energy to escape the galaxy; indeed, some of it returns to the gas reservoir of the galaxy, increasing its metallicity.

In Sec. 2, we will present the dataset and the techniques we used, then, in Sec. 3, we will develop the concepts introduced here in a more mathematical way and present our results. Finally, in Sec. 4, we will discuss our results and draw conclusions from them.

2 METHODS

This work is based on a subset of the **Sloan Digital Sky Survey** (SDSS) dataset. In particular, we study 92483 galaxies with redshift < 0.08 ($z_{\rm mean} \simeq 0.054$), for which we have five-band photometric data. This data may seem too sparse to obtain a valuable estimate of the SFR, but we have been able to achieve this by employing a powerful library called **CIGALE** (Code Investigating GALaxy Emission). It generates a grid of model parameters and fits the photometric data with each model, selecting the best one through a Bayesian approach based on likelihood maximization. The way in which CIGALE builds its models is quite sophisticated, as it takes into account many factors, such as:

- **Star formation history (SFH):** describes how the SFR changes over time.
- **Initial mass function (IMF):** describes the mass distribution of newly-formed stars.
- **Stellar population synthesis (SPS):** describes the spectrum emitted by a certain stellar population at a given time. This population is formed according to a SFH, an IMF, and an initial metallicity. It takes into account how stars evolve over time, as a function of mass and metallicity.
- **Dust attenuation:** describes how the light emitted by stars is absorbed and re-emitted by galactic dust.
- **Nebular emission:** describes the light emitted by ionized gas regions within the galaxy.

We choose (1) to model SFH with a double exponential, (2) to employ the IMF by Chabrier (2003), (3) to model SPS according to Bruzual & Charlot (2003), (4) to model dust attenuation with Calzetti et al. (2000) and Leitherer et al. (2002) formulae, and (5) to take into account nebular emission. This is just a brief description of how CIGALE works, we suggest checking the original paper (Boquien et al. 2019) for the details.

Besides SFR, CIGALE provides a series of valuable estimates of galactic quantities, such as $M_{\rm star}$ and age. In this work, we will focus on the sSFR versus $M_{\rm star}$ plane. We can approximately divide the two populations by drawing a line corresponding to the minimum of the sSFR distribution, as can be seen in Fig. 1. In our case, we obtain $\mathrm{sSFR}_{\rm threshold} = 5.73 \times 10^{-11}\,\mathrm{yr}^{-1}$. Finally, CIGALE also provides uncertainties for its estimates; we have decided to neglect them in this exploratory analysis, but they should be taken into account to check the significance of our results.

3 RESULTS

3.1 Mathematical introduction

We would like to derive a mathematical relation between the sSFR and $M_{\rm star}$. Since the raw material for star formation is gas, we expect the SFR to be proportional to the amount of available gas, i.e., $\mathrm{SFR} \propto M_{\rm gas}^{\alpha}$, where the proportionality constant must have the dimensions of inverse time. We assume the linear relation originally found by Kennicutt (1998):

$$\mathrm{SFR}\left(M_{\rm gas}\right) \simeq \frac{\epsilon}{\tau_{\rm dyn}} M_{\rm gas} \doteq \epsilon' M_{\rm gas}, \tag{2}$$

where $\epsilon \simeq 0.02$ is an efficiency parameter and $\tau_{\rm dyn}$ is the dynamical time, which is given by:

$$\tau_{\rm dyn} = 2 \times 10^7\,\mathrm{yr} \left(\frac{R_{1/2}}{4\mathrm{kpc}}\right) \left(\frac{v_{\rm circ}}{200\mathrm{km\ s}^{-1}}\right)^{-1}. \tag{3}$$

However, for simplicity we assume $\tau_{\rm dyn} = 2 \times 10^7\,\mathrm{yr}$, because it has only a mild impact on the result.

In general, the time evolution of $M_{\rm gas}$ can be described by the following differential equation:

$$\frac{dM_{\rm gas}(t)}{dt} = \dot{M}^{\rm in}_{\rm gas}(t) - \dot{M}^{\rm out}_{\rm gas}(t) - (1-R)\,\mathrm{SFR}(t), \tag{4}$$

where R is the fraction of gas that undergoes the star formation process, but then returns to the gas reservoir due to stellar winds and supernovae. As mentioned in Sec. 1, the gas outflow depends on a series of processes, but we only consider the most important: Type IIA supernovae. Their contribution can be simply written as:

$$\dot{M}^{\rm out}_{\rm gas}(t) \simeq \eta \mathrm{SFR}(t), \tag{5}$$

where η is the supernovae feedback parameter, that, in general, depends on time. Therefore, eq. 4 becomes:

$$\frac{dM_{\rm gas}(t)}{dt} = \dot{M}^{\rm in}_{\rm gas}(t) - (1+\eta-R)\,\frac{\epsilon}{\tau_{\rm dyn}} M_{\rm gas}. \tag{6}$$

Describing gas inflow is a little more complicated, as it depends on $M_{\rm halo}$. In general, we can write:

$$\dot{M}^{\rm in}_{\rm gas}(t) = \xi\, \dot{M}^{\rm in}_{\rm halo,gas}(t) = \xi\, f_{\rm gas}\, \dot{M}^{\rm in}_{\rm halo}(t), \tag{7}$$

where we can assume $f_{\rm gas} = 0.15$ and $\xi \in [0,1]$ is a function related to the cooling efficiency discussed in Sec. 1. The simplest possible form for ξ is a step-function:

$$\xi_{\rm step} = \begin{cases} 0 & \text{If } \tau_{\rm cool} > \tau_{\text{free-fall}}\text{ , i.e. , } M_{\rm halo} \notin \left(M_{\rm halo,min}\text{ , }M_{\rm halo,max}\right) \\ 1 & \text{If } \tau_{\rm cool} < \tau_{\text{free-fall}}\text{ , i.e. , } M_{\rm halo} \in \left(M_{\rm halo,min}\text{ , }M_{\rm halo,max}\right) \end{cases} \tag{8}$$

$\dot{M}^{\rm in}_{\rm halo}(t)$ is still unknown to us, but we can assume a relation obtained from the **Millennium Simulation** (McBride et al. 2009):

$$\dot{M}^{\rm in}_{\rm halo}(z) = 42 M_\odot \mathrm{yr}^{-1} \left(\frac{M_{\rm halo}}{10^{12} M_\odot}\right)^{1.127} (1+1.17z)\sqrt{(1+z)^3\Omega_m + \Omega_\Lambda}, \tag{9}$$

where we can assume $\Omega_m = 0.3$ and $\Omega_\Lambda = 0.7$.

There is still an unknown quantity, $M_{\rm halo}$. We can estimate it by numerically inverting the empirical relation found by Moster et al. (2012):

$$M_{\rm star}\left(M_{\rm halo}\right) = 2NM_{\rm halo}\left[\left(\frac{M_{\rm halo}}{M_1}\right)^{-\beta} + \left(\frac{M_{\rm halo}}{M_1}\right)^{\gamma}\right]^{-1}, \tag{10}$$

where N, β, γ, and M_1 are coefficients that can be found in the original paper and that depend on redshift (we assume $z_{\rm mean} \simeq 0.054$). We can use this relation to transform eq. 1 into an efficient-cooling condition on $M_{\rm star}$:

$$M_{\rm star} \in \left(M_{\rm star,min} = 10^{4.3} M_\odot\text{ , }M_{\rm star,max} = 10^{10.1} M_\odot\right). \tag{11}$$

As shown in Fig. 2, most passive galaxies ($\approx 64\%$) exceed $M_{\rm star,max}$, and therefore, we expect them to have $\dot{M}^{\rm in}_{\rm gas} \approx 0$. Moreover, we can see that passive galaxies are, on average, much older than star-forming ones. This suggests that the former may have already depleted most of their gas, and therefore there is little left that can be ejected out of the galaxy by supernovae (i.e., $\eta \approx 0$). For these reasons, we can approximate the passive galaxies with a closed-box model, in which there is no exchange of gas between the galaxy and its halo. On the other hand, star-forming galaxies should be modeled with an open-box model, as we expect them to both accrete and eject gas. In the next sections, we will try to describe the two populations using one model for each, ideally merging into a single model with a sharp transition at $M_{\rm star,max}$.

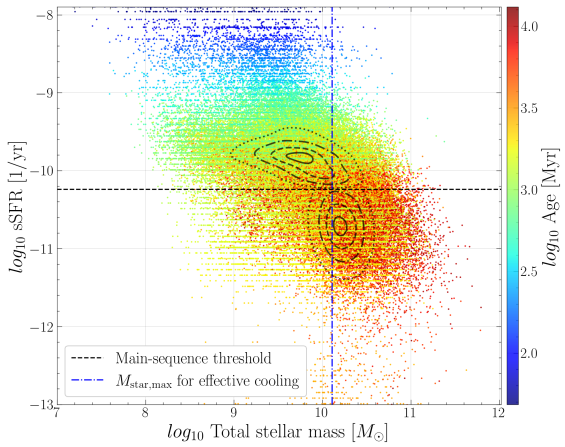

Figure 2. 2D scatter-plot of sSFR versus M_{star} for our dataset, where the color is proportional to the age. The black dashed line separates the main sequence from passive galaxies. The blue dash-dot line indicates $M_{star,max}$. The 25, 50, 75, and 95% contours of both populations are shown.

3.2 Open-box model at equilibrium for star-forming galaxies

We can solve eq. 6 analytically in three special cases: when one of the two RHS terms is negligible with respect to the other, or when they are equal. In this last case, M_{gas} is constant over time, and therefore this is an equilibrium solution. Since we want to describe star-forming galaxies with a model in which both accretion and ejection of gas are relevant, we consider the equilibrium case. From eq. 6, we get:

$$M_{gas}^{eq}(t) = \frac{\dot{M}_{gas}^{in}(t)}{(1+\eta-R)\epsilon'} \Rightarrow sSFR^{eq}(M_{star}) = \frac{\dot{M}_{gas}^{in}(M_{star})}{1+\eta-R}\frac{1}{M_{star}}, \quad (12)$$

where $\dot{M}_{gas}^{in}(M_{star})$ is given by eqs. (7) to (10), with $z_{mean} \simeq 0.054$, while η and R are free parameters of the model. Our result is represented by the red line in Fig. 3. We set $\eta = 0.9$ and $R = 0.4$ to get the model as close as possible to the median of the star-forming galaxies, represented by the black solid line.

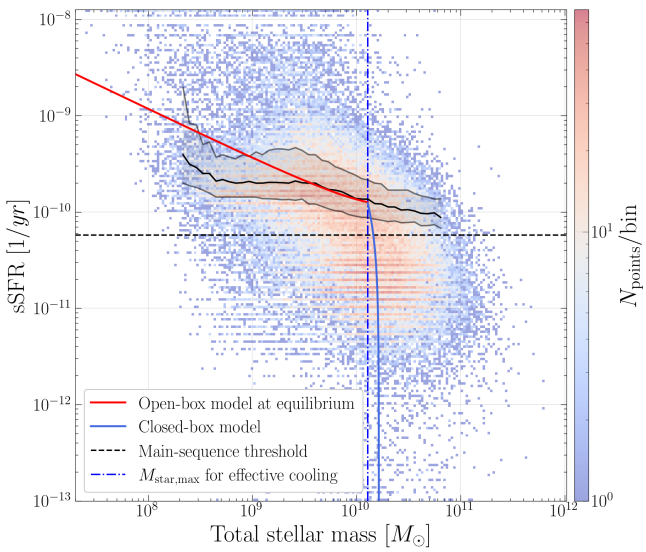

Figure 3. 2D histogram of sSFR versus M_{star} for our dataset. The black dashed line separates the main sequence from passive galaxies. The black solid line is the median of the main sequence. The blue dash-dot line indicates $M_{star,max}$. The red solid line is the open-box model at equilibrium. The blue solid line is the closed-box model.

3.3 Closed-box model for passive galaxies

The closed-box model sets $\dot{M}_{gas}^{in} = 0$ and $\eta = 0$ in eq. 6, which then becomes trivial:

$$M_{gas}(t) = M_{gas}(t_0)\exp\{[-(1-R)\epsilon'(t-t_0)]\}, \quad (13)$$

where t_0 is the time at which M_{star} exceeds $M_{star,max}$ and, in our assumption, the closed-box model becomes valid. We can compute the SFR from eq. 2 and integrate it, from t_0 to t, to obtain M_{star}:

$$\begin{aligned} M_{star}(t) =& (1-R)\int_{t_0}^{t} \text{SFR(t')dt'} = \\ =& M_{star}(t_0) + M_{gas}(t_0)\,\{1-\exp[-(1-R)\epsilon'(t-t_0)]\}\,. \end{aligned} \quad (14)$$

Since we want to write the SFR as a function of M_{star}, we can substitute the exponential of eq. 13 with the expression obtained by inverting eq. 14:

$$\begin{aligned} M_{gas}(M_{star}) =& M_{gas}(t_0)\left[1-\frac{M_{star}-M_{star}(t_0)}{M_{gas}(t_0)}\right] = \\ =& M_{gas}(t_0) - M_{star} + M_{star}(t_0) \doteq \\ \doteq& M_{total}(t_0) - M_{star}, \end{aligned} \quad (15)$$

which is not surprising for a closed-box. The last step consists of substituting eq. 15 into eq. 2 and, finally, dividing by M_{star}:

$$sSFR(M_{star}) = \epsilon'\left(\frac{M_{total}(t_0)}{M_{star}} - 1\right). \quad (16)$$

We approximate $M_{star}(t_0)$ with $M_{star,max}$, since this is the threshold past which we consider our closed-box model as valid. $M_{gas}(t_0)$ is a free parameter, because we do not know anything about it. We consider $M_{gas}(t_0) = M_{star,max}/8$. The other free parameters are $\epsilon = 0.02$ and $\tau_{dyn} = 2\times10^7$yr, as the final formula is independent on R. The final result is given by the solid blue line in Fig. 3, which drops extremely fast as M_{star} increases.

3.4 Numerical integration

In the previous derivation of $sSFR(M_{star})$ in the open-box model, we considered inflow and outflow of gas to be equal. We can relax this strong assumption by switching to a numerical approach. In particular, we can integrate eq. 6 over infinitesimal time steps, from the formation time (t_{form}) to the time of observation. This allows us to take into account the time evolution of $\dot{M}_{gas}^{in}$ (cf. eq. 9) and τ_{dyn}, which actually goes as $(1+z)^{-3/4}$.

We generate a population of galaxies that formed at different times $t_{form,i}$, all with an initial halo mass $M_{halo}(t_{form,i}) = 5\times10^8 M_\odot$. Then, we integrate M_{halo} (eq. 9), M_{gas} (eqs. (6) to (8)), and M_{star} (integral of SFR, given by eq. 2) over infinitesimal time steps, obtaining values of sSFR and M_{star} at the observational time, which can be compared to our data. The result obtained by employing ξ_{step} is shown in Fig. 4, where we set $\eta = 4$ and $R = 0.1$. Even though the most important aspect here is the functional behavior, we should point out that we had to fix a vertical offset, of unknown nature, by multiplying the y-values by ≈ 4.

We can relax one more assumption by employing a model of ξ that is more physically meaningful than a step function. For example, Davé et al. (2011) developed a sophisticated model, taking into account many physical processes that influence accretion of gas from the halo:

$$\xi_{Davé} = \xi_{photo}\,\xi_{quench}\,\xi_{grav}\,\xi_{winds}, \quad (17)$$

where (1) ξ_{photo} describes the photoionization heating that suppresses gas inflow at low masses, (2) ξ_{quench} models the quenching

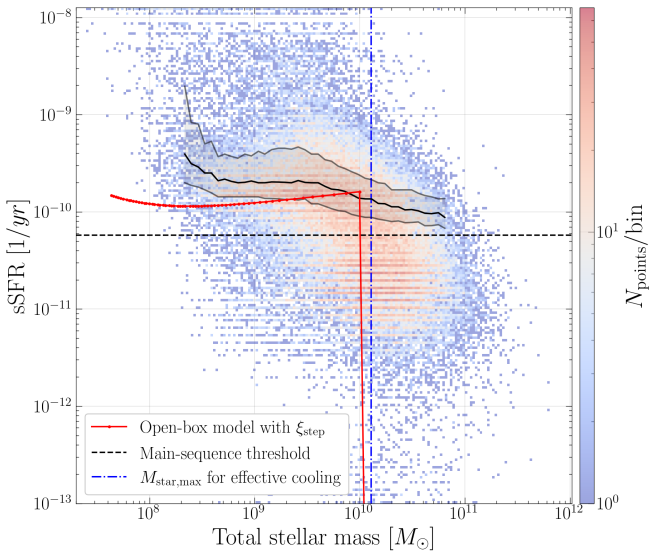

Figure 4. 2D histogram of sSFR versus $M_{\rm star}$ for our dataset. The black dashed line separates the main sequence from passive galaxies. The black solid line is the median of the main sequence. The blue dash-dot line indicates $M_{\rm star,max}$. The red solid line is the numerical open-box model with $\xi_{\rm step}$.

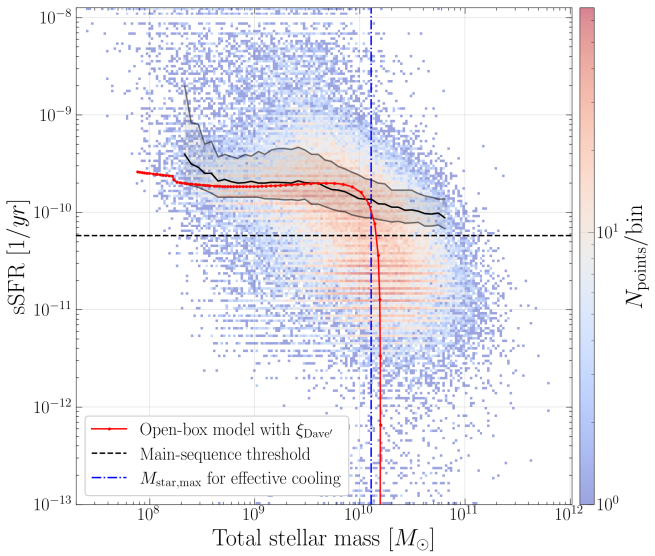

Figure 5. 2D histogram of sSFR versus $M_{\rm star}$ for our dataset. The black dashed line separates the main sequence from passive galaxies. The black solid line is the median of the main sequence. The blue dash-dot line indicates $M_{\rm star,max}$. The red solid line is the numerical open-box model with $\xi_{\rm Davé}$.

effect of SMBHs in massive halos, (3) $\xi_{\rm grav}$ is related to gas heating due to the formation of gravitational structures at high masses, and (4) $\xi_{\rm winds}$ describes the quenching caused by winds at low masses. The functional form of each of them can be found in the original paper. The resulting $\xi_{\rm Davé}$ drops more gently than $\xi_{\rm step}$ and this reflects on the final result, displayed in Fig. 5, that seems a continuous function of $M_{\rm star}$ and fits the data more accurately. In this case, we used $\eta = 1.3$ and $R = 0.4$, that are more similar to the values of Fig. 3. Even this time, we had to fix an unexpected vertical offset (multiplied the y-values by ≈ 7).

4 DISCUSSION

The results in Figs. 3 and 5 are remarkably similar for $M_{\rm star} > M_{\rm star,max}$, rapidly dropping as $M_{\rm star}$ increases. This is not surprising, as in both cases the inflow of gas is almost zero for massive galaxies ($\xi_{\rm step} = 0$ for the former, $\xi_{\rm Davé} \approx 0$ for the latter). The main difference between the two cases is the presence of gas outflow: we set $\eta = 0$ for the analytical case and $\eta = 1.3$ for the numerical case, which causes a small outflow effect in the passive region, as $\dot{M}_{\rm gas}^{\rm out}$ is also proportional to the SFR (cf. eq. 5). We could further generalize the time evolution by implementing $\eta = \eta(t)$ and $R = R(t)$ according to stellar physics and galaxy evolution. For example, we expect η to decrease over time, as old galaxies have already converted most of their gas into stars, and therefore they have very little gas left to be ejected. Another difference is that, while for the analytical case $M_{\rm gas}(t_0)$ is a free parameter we have to choose, in the numerical case it is simply a result of the evolution from the formation time up to when $\xi_{\rm Davé} \approx 0$ (i.e., when $M_{\rm star}(t) \approx M_{\rm star,max}$).

On the other hand, the results are quite different for actively star-forming galaxies, i.e., for $M_{\rm star} < M_{\rm star,max}$, even though both of them correctly fit at least a region of the main sequence. In the analytical case, we had to assume $\dot{M}_{\rm gas}^{\rm in} = \dot{M}_{\rm gas}^{\rm out}$ at the time of observation, in order to solve the differential equation. On the contrary, numerical evolution is more general, as outflow and inflow can change freely. For this reason, we think that the numerical result is more trustworthy.

Overall, all our models display a more or less constant sSFR($M_{\rm star}$) in the star-forming region, that rapidly drops as soon as we enter the passive region, and this is the behavior we expected. The values we found for R, η, ϵ, and $\tau_{\rm dyn}$ should be taken with a grain of salt, since they are almost all degenerate with one another. Finally, the fact that, in the numerical case, we have been forced to fix a vertical offset by hand remains an unsolved problem.

We could relax further approximations by considering more outflow processes. Even though Type IIA supernovae are the dominant driver for gas ejection, AGN emission and ram-pressure stripping in dense environments are both relevant processes that should be taken into account. For example, we could add a $\dot{M}_{\rm gas}^{\rm out,AGN} \propto M_{\rm SMBH}$ term to the observed galaxies that host an AGN. We can identify these galaxies by looking at the relative strength of forbidden emission lines, since they require excitation from high-energy radiation, and AGNs are the best candidates for emitting it in large quantities. A first attempt in this direction is shown in Fig. 6, where we considered a discriminant function (Kauffmann et al. 2003b) in the plane of log $\left([\mathrm{OIII}]\,\lambda5007/H_\beta\right)$ versus log $\left([\mathrm{NII}]\,\lambda6584/H_\alpha\right)$. It is clear that most AGNs appear in massive galaxies, and therefore their sSFR($M_{\rm star}$) should drop even faster.

AGN emission is just one of the many assumptions we could relax, as galaxy evolution is an extremely complicated topic. Introducing ram-pressure stripping and interactions between galaxies in our model would be even more complicated. For example, it is not obvious whether an interaction between two neighboring galaxies would either stimulate or quench their star-formation processes. Note that these additional outflow terms may not directly depend on the SFR, and therefore they could remain relevant even for old, passive galaxies, that would not be closed-boxes anymore.

5 SUMMARY

In conclusion, we discovered that it is indeed possible to describe the sSFR($M_{\rm star}$) bimodality in galaxies at low redshift through simple models. In particular, we have been able to model young, star-forming

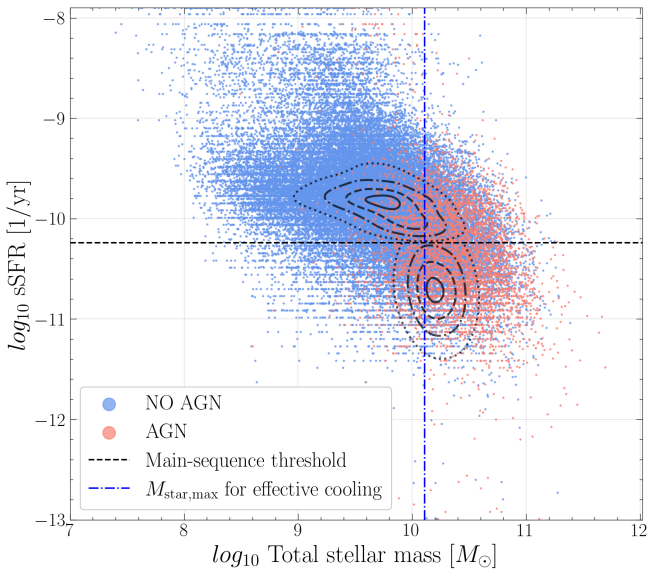

Figure 6. 2D scatter-plot of sSFR versus M_{star} for our dataset, where the color discriminates AGNs. Only the galaxies with a SNR high enough are displayed. The black dashed line separates the main sequence from passive galaxies. The blue dash-dot line indicates $M_{\mathrm{star,max}}$.

galaxies as open-boxes, which constantly exchange gas with the surrounding environment. The inflow of gas is dominated by the halo, while the outflow depends on a series of processes, such as Type IIA supernovae, AGN emission, and ram-pressure stripping, which, in turn, depend on mass, age, and even the galactic environment. Concerning old, mostly passive galaxies, in first approximation they can be modeled as closed-boxes, even though they may be ejecting some gas through processes that do not depend on the formation of new stars.

The models we developed can be enriched by adding further physical processes, such as the already mentioned AGN emission and ram-pressure stripping, but also by refining those that are already present. For example, we assumed η and R to be fixed constants, but they should be modeled according to physical processes instead. Another strong assumption we did concerns the interval in which gas cooling is efficient, which has a huge impact on the final results.

REFERENCES

Boquien M., Burgarella D., Roehlly Y., Buat V., Ciesla L., Corre D., Inoue A. K., Salas H., 2019, Astronomy and Astrophysics, 622, A103
Bruzual G., Charlot S., 2003, MNRAS, 344, 1000–1028
Calzetti D., Armus L., Bohlin R. C., Kinney A. L., Koornneef J., Storchi-Bergmann T., 2000, The Astrophysical Journal, 533, 682–695
Chabrier G., 2003, PASP, 115, 763–795
Davé R., Finlator K., Oppenheimer B. D., 2011, MNRAS, pp no–no
Kauffmann G., et al., 2003a, MNRAS, 341, 54–69
Kauffmann G., et al., 2003b, MNRAS, 346, 1055–1077
Kennicutt Jr. R. C., 1998, The Astrophysical Journal, 498, 541–552
Leitherer C., Calzetti D., Martins L. P., 2002, The Astrophysical Journal, 574, 114
McBride J., Fakhouri O., Ma C.-P., 2009, MNRAS, 398, 1858–1868
Mo H., van den Bosch F. C., White S., 2010, Galaxy Formation and Evolution. Cambridge University Press
Moster B. P., Naab T., White S. D. M., 2012, MNRAS, 428, 3121–3138